Effect of Convective Heat Transfer and Phase Change on the Stability of Aluminium Smelting Cells

This paper focuses on two aspects of smelting operation that are highly dependent on the rate of heat transfer in the molten bath. As a consequence of the elevated temperature and the corrosive nature of the fluoride mixture, the cell sidewalls are designed so that some electrolyte will freeze onto them, protecting the carbon from erosion and at the same time insulating the cell against excessive heat loss. The thickness and dynamic variation of this frozen ledge are determined by the convective heat transfer from the bath to the freeze surface.

Another situation where the rate of convective heat flow exerts a subtle influence is the dissolution of aluminium oxide powder in the bath. The localized feeding of large quantities of the powder causes transient electrolyte freezing on some of the added material, hindering its dissolution and causing the formation of an alumina sludge below the molten aluminium pad.

M. P. Taylor, B. J. Welch, R. McKibbin
School of Engineering,
University of Auckland
Auckland, New Zealand

Introduction

The electrochemical reduction of aluminium oxide to aluminium is performed in a cryolite-based electrolyte contained within carbon-lined cells. Because ionic mobility is required for the electrolysis reaction, it is necessary that the ohmic heat generated between the anode and cathode be sufficient to maintain the electrolyte above its melting point—that it be "superheated" in the parlance of industry. However the degree of superheat is low in practice and varies continuously as a result of electrochemical and energy changes associated with the depletion, addition, and dissolution of the feedstock, alumina (Taylor et al. 1984).

The background to this study is the dynamic variation and thermal instability associated with smelting cell operation. This instability is strongly linked with electrochemical inefficiency in the process (Kent, 1970) and actual cell degradation (Taylor et al., 1983a). Its basic cause is the batchwise addition and removal of reactants and products in the reaction. These actions give rise to rapid shifts in the energy balance, although electrolysis is occurring continuously in the molten mixture. The net effect is a cyclic fluctuation in operating parameters (Schmidt-Hatting, 1975), and process control becomes a question of limiting the amplitude of the cycles to an acceptable level. The present paper is indirectly concerned with the determination of a stability threshold for these variations, although its bias is mainly experimental. The approach has been to investigate a fundamental characteristic of a fusible material elevated above its melting point: its tendency to give up sensible heat to the surroundings and to freeze. If the evolution of latent heat accompanying this phase change meets a temporary energy demand such as the preheating and dissolution of a cooler material added to the molten salt, it is probable that the freezing will be followed by remelting of the solid phase. On the other hand, a steady heat loss from the walls containing the melt (as occurs in a smelting cell where the heating is developed by the passage of current in the electrolyte) may result in a permanent frozen layer adhering to these sidewall surfaces (Grjotheim and Welch, 1980).

In both cases, the quantity of material that freezes and the speed at which freezing and melting take place, depend heavily on the rate of sensible heat transport from the bulk of the liquid to the phase change interface. When a large quantity of alumina powder is dropped into the molten electrolyte, the heat capacity of the cooler solid, combined with its endothermic enthalpy of dissolution, gives rise to localized cooling of melt in the vicinity of the addition (Bratland et al., 1976). Subsequent freezing of cryolite around aggregates of undissolved alumina (Jain et al.,

1983a) could block the dissolution process, and if these aggregates are large enough (Keller, 1984) a sludge of alumina and solid or saturated liquid electrolyte will sink into the liquid aluminium, where its dissolution kinetics are unfavorable. The existence of this slow-dissolving sludge is well known in smelting cells (Thonstad et al., 1980) since it is a primary cause of unstable voltage oscillations and contributes to poor heat balance in the operation.

The integrity of a cell is threatened in a different way when the frozen ledge of cryolite adhering to the sidewalls is allowed to melt off or is not in fact formed at cell start-up. Prolonged exposure of the carbonaceous material to the erosive fluoride melt and swirling aluminium pad below causes a steady decline in the thickness of the walls and often leads to premature failure of the cell (Peacey and Medlin, 1979). In practice the thermal resistance of the walls and the superheat of the electrolyte are the *controlling* parameters for frozen ledge formation, but the prediction of their design values and the allowance of a "safety" thickness of ledge against fluctuations in the superheat requires accurate knowledge of the heat transfer coefficient at the surface of the solid layer.

The convective heat transfer between the molten and frozen phases is therefore a process worthy of experimental clarification since it is one mechanism by which the process dynamics influence the operating stability of the cell. In the case of frozen ledge formation, *in situ* measurements of electrolyte superheat and cell heat balance have been reported earlier (Taylor et al., 1983a). Together with one-dimensional heat flow modeling through the side wall, these measurements have allowed the application of steady and transient heat transfer coefficients, reviewed here, in a computer simulation of the variation in ledge thickness at the position of minimum coverage on the wall (Taylor et al., 1983b). The problem of alumina sludging is less amenable to exact analysis. The mechanism proposed in this paper perceives sludging as a consequence of heat transfer control during the dissolution process. On the basis of transient heat flux measurements made during block quenching experiments, frozen electrolyte encapsulation of alumina aggregates above a critical size has been predicted, although whether these larger particles are formed through agglomeration of individual grains or by fragmentation of the surface crust during feeding is still unclear.

Experimental

To date the only physical evidence of heat transfer control in the alumina dissolution process is the difference between the dissolution time of a microscopically observed grain (Noguchi et al., 1983) (60–120 s) and that of a quantity of alumina powder dropped into the electrolyte (Jain et al., 1983b; Gerlach et al., 1974) (300–600 s). Confirmation of the mechanism requires visual observation of the frozen layer and quantitative determination of the heat transfer rate during the phase change process. Since neither of these is possible during the actual dissolution of alumina powder, larger cylindrical graphite blocks were plunged into a known mass of electrolyte and the thermal effects of the quench were observed. This procedure is somewhat similar to drop calorimetry and has been used to study the liquid vaporization and boiling heat flux at the surface of a nickel cylinder quenched from 1,073 K (Archambault and Chevrier, 1977). The graphite blocks used here were inert with respect to the electrolyte and had measurable thermal responses. Thus,

Table 1. Description of Cylinder Geometry for the Three Blocks Tested

Block Mass kg × 10^3	Radius, r m × 10^3	Height, m × 10^3	$R = V_c/A_c$ m × 10^3	Shape Factor, S
15.0	14.09	14.92	3.62	1.20
25.0	14.05	24.20	4.45	1.15
41.0	17.78	24.38	5.14	1.16

although the experiments in no way simulated alumina dissolution, the energy demand of each block was a simple function of its embedded thermocouple temperatures, while its removal at intermediate intervals after immersion allowed visual inspection and measurements of the frozen electrolyte adhering to its surface. The quenching experiments were performed using an electrolyte of typical smelter composition (7 wt. % CaF_2, 2.5 wt. % Al_2O_3, NaF:AlF_3 = 1.35 wt. ratio) with a superheat of 16 K above the liquidus temperature (determined by cooling curve analysis to be 1,241 ± 1 K). Three cylinders were tested in this study and these are described in Table 1.

The equivalent radius of each cylinder is its volume to surface area ratio:

$$R = V_c/A_c \tag{1}$$

while the shape factor, S, is defined here as the surface area to volume ratio referenced to that of a sphere having the same volume:

$$S = A_c/A_s \left[= \left(\frac{3V_c}{3\pi}\right)^{1/3} \left(\frac{1}{3R}\right) \right] \tag{2}$$

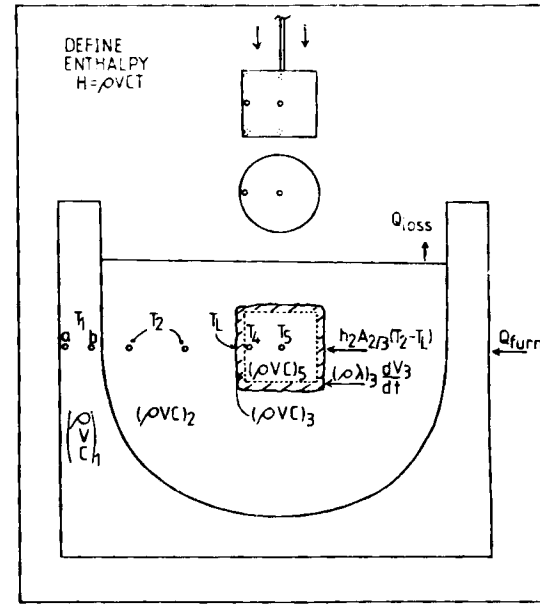

Figure 1. Diagram of experimental set-up, showing lumped heat capacities, major heat flows, and approximate positions of thermocouples.

1. Containment crucible
2. Molten electrolyte
3. Frozen electrolyte
4. Surface of immersed cylinder
5. Body of immersed cylinder

Type K chromel-alumel thermocouples were employed to monitor the thermal history of the system and each was read about 500 times during the course of an experiment by a cold junction, compensated digital voltmeter (accuracy 1×10^{-5} V or 0.25 K) which was interfaced with an HP9826 computer and an HP3497A data acquisition system. The positions of the thermocouples and the locations of the major heat flows and thermal capacities in the experimental set-up are given in Figure 1.

Reproducibility of the quench procedure, and the thermal response to it, was adequate when a number of tests were carried out. For some of the experiments six thermocouples were embedded in the quenched cylinder, one at the center and five at selected locations near the surface. However it was found that a central (T_5) and a radial (T_4) temperature measurement at mid height in the cylinder provided a sufficiently accurate record of its thermal history. Reconstruction of the material adhering to the cylinders at each intermediate quenching operation allowed visualization of the growth and decay of the frozen layer. The reconstructed freeze coverings for the 0.015 and 0.041 kg blocks are shown in Figure 2.

Analysis

Mathematical analysis of the quenching problem has been reported for vaporization around the heated nickel cylinder (Archambault and Chevrier, 1977). However this solution employs the transient conduction equation inside the cylinder, assuming both radial heat flow within it and a spatially uniform heat flux at the surface. Unfortunately neither of these assumptions is applicable during complete immersion of a short cylinder since a vertical as well as a radial temperature gradient exists in the block, while reference to Figure 2 indicates that the bottom of the freeze layer melts off the cylinder first. Therefore an energy conservation approach was preferred in this problem.

Since the thermal responses of the system components are measured directly, a differential energy balance based on their lumped heat capacities (subscripts *1* to *5* in Figure 1) should isolate the convective heat flows between them as well as the latent fusion energy supply to the graphite cylinder. The overall heat balance must include the response of the furnace, $Q_{\text{furn}}(t)$, to the quenching operation as well as the steady heat loss from the surface of the electrolyte, $Q_{\text{loss}}(t)$:

$$Q_{\text{furn}}(t) - Q_{\text{loss}}(t) = \frac{dH_1}{dt} + \frac{dH_2}{dt} + \frac{dH_3}{dt} + \frac{dH_5}{dt} - \lambda_3 \frac{d}{dt}(\rho_3 V_3) \quad (3)$$

In this model the enthalpy, H, of each material is a function of its density, ρ, its heat capacity, C, its volume, V, and its temperature:

$$H = \rho V C T \quad (4)$$

Substitution of the enthalpy definition, Eq. 4, into Eq. 3 yields a first-order differential equation in $V_3(t)$, the volume of frozen material present on the immersed cylinder. Also, since the extra heat input from the furnace, $Q_{\text{furn}} - Q_{\text{loss}}$, is a prescribed function of the time after the furnace temperature falls below its control point, solution of this equation should give the mass of

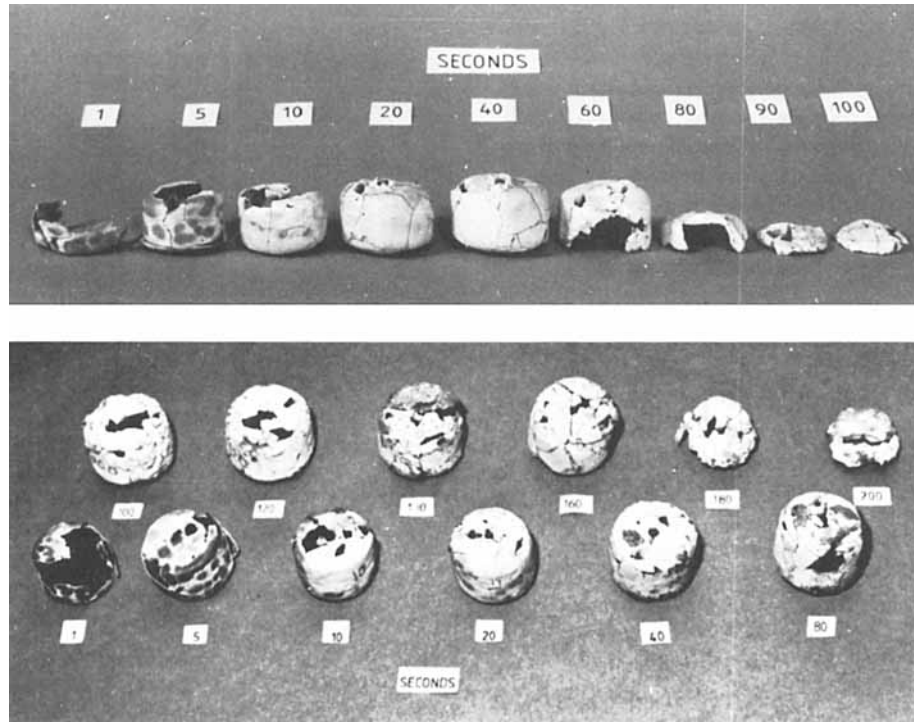

Figure 2. Frozen electrolyte reconstrucations.
A. 0.015 kg graphite cylinders
B. 0.041 kg graphite cylinders

freeze, $\rho_3 V_3(t)$, at any time after the quenching operation:

$$\rho_3\left[-\lambda_3 - C_2T_2 + C_3\frac{(T_L+T_4)}{2}\right]\cdot\frac{dV_3}{dt}(t) + \frac{\rho_3C_3}{2}\frac{dT_4}{dt}\cdot V_3(t) = (Q_{furn} - Q_{loss})(t) - \frac{\rho_1V_1C_1}{2}\left(\frac{dT_{1a}}{dt}+\frac{dT_{1b}}{dt}\right) - \rho_2V_2C_2\frac{dT_2}{dt} - \frac{\rho_5V_5C_5}{3}\left(2\frac{dT_4}{dt}+\frac{dT_5}{dt}\right) \quad (5)$$

Equation 5 uses Lagrangian interpolation polynomials to calculate the enthalpy of the cylinder in terms of T_4 and T_5, while an arithmetic average of the phase change temperature, T_L, and the surface temperature of the cylinder, T_4, is employed to determine the freeze enthalpy. Other simplifications are achieved by the evaluation of average density and heat capacity values for the graphite cylinder and by invoking the conservation of mass constraint for the electrolyte:

$$\rho_3 dV_3 = -\rho_2 dV_2 \quad (6)$$

Individual heat balances on the cylinder and the frozen layer allow the convective heat flow between the melt and freeze to be computed from $V_3(t)$ above:

$$h_2A_{2/3}(T_2 - T_L) = \frac{\rho_5V_5C_5}{3}\left(\frac{2dT_4}{dt}+\frac{dT_5}{dt}\right) + \frac{\rho_3C_3}{2}\frac{dT_4}{dt}V_3(t) + \rho_3\left[-\lambda_3 + C_3\frac{(T_4+T_L)}{2} - C_2T_2\right]\cdot\frac{dV_3}{dt}(t) \quad (7)$$

A difficulty arises in the solution of both Eq. 5 and Eq. 7 when a value of T_L must be assigned since, during rapid freezing processes, solute rejection of the liquid is unable to occur (Thonstad and Rolseth, 1983) and the phase change temperature is therefore closer to the double solubility (pseudoeutectic) line (Lee et al., 1984) than the liquidus point for the actual electrolyte composition. However, at the instant of complete remelting of the frozen layer, the skin of the graphite block must attain the temperature of the melting front. This fact will be used to determine T_L in the quenching experiments.

Results

In Figure 3 the frozen electrolyte-time profiles calculated from Eq. 5 are presented. Superimposed on these computer predictions are the experimentally determined freezing data, some of which have been reconstructed in Figure 2. Correspondence between experiment and theory is good considering the simplicity of the heat balance model and the random error inherent in the quenching procedure. In general the model underpredicts the initial rate of freezing slightly but is probably more representative of the process in the melting regime than the actual data, which exhibit considerable scatter due to the irregular way in which the final remelting occurs. As shown by Figure 2, the lower face and sides of the freeze covering disappear first, indicating enhanced heat transfer between the bottom of the cylinder and the crucible. This may be the result of cellular convection patterns induced by the adverse temperature gradient between the two horizontal surfaces (Tankin and Farhadieh, 1971).

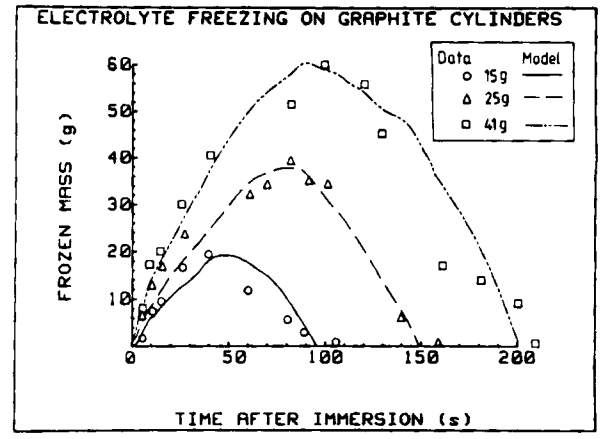

Figure 3. Theoretical and experimental frozen electrolyte mass-time profiles of the three graphite cylinders.

The phase change process can be generalized for an object of arbitrary size and shape quenched in this electrolyte at the same superheat. The immersion time of the object is nondimensionalized in the Fourier number:

$$Fo = \frac{\alpha_5 t}{R^2} \quad (8)$$

where α_5 is the thermal diffusivity of the graphite cylinder. The frozen mass profile may be expressed as the ratio of the latent heat supply, E_s, to the total energy demand, E_d, of the block and freeze layer, multiplied by the shape factor ($S = 1.0$ for a sphere):

$$S\cdot(E_s/E_d) = S\cdot\frac{\rho_3V_3(t)\lambda_3}{[\rho_5V_5C_5 + \rho_3V_3(t)C_3](T_L - T_o)} \quad (9)$$

where T_o is the temperature of the object before the quenching operation. Figure 4 shows this dimensionless plot for the three blocks tested and it seems that the extent and the tenacity of the electrolyte encapsulation is a predictable function of the heat capacity and shape of the quenched body.

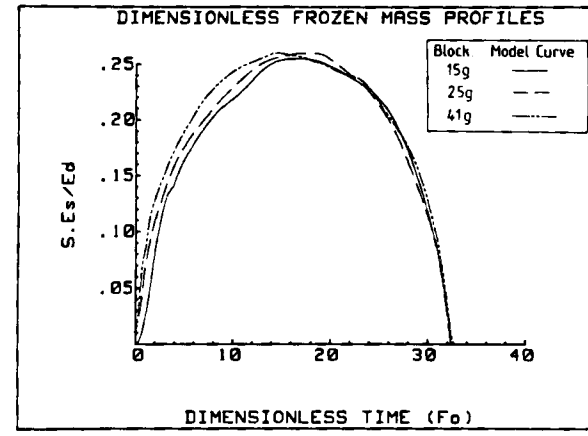

Figure 4. Dimensionless frozen electrolyte mass-time profiles defined by Eqs. 8 and 9.

Application to Alumina Dissolution

If the thermal capacity of the cooler alumina was the only impetus for heat transfer during the dissolution process, possible encapsulation of alumina aggregates in frozen electrolyte could be predicted using the simple correlation given in Figure 4. However, after the first thermal shock of the alumina addition, the effect of transient conduction inside the solid is replaced by the enthalpy demand of dissolution at the surface. If the initial dissolution rate of a grain or an agglomeration of grains cannot be supported by the sensible heat flow to the surface of the solid, localized cooling and freezing of electrolyte must occur. Assuming an initial, unhindered bulk rate of disappearance of the added material, $dM_{Al_2O_3}/dt$, and an average particle radius, $r_{Al_2O_3}$, the criterion for continued dissolution without heat transfer control can be written:

$$h_2(T_2 - T_{Al_2O_3}) = \frac{\Delta H_{\text{dissolution}}}{(3M_{Al_2O_3})} \cdot \rho r_{Al_2O_3} \cdot \frac{dM_{Al_2O_3}}{dt} \quad (10)$$

where $M_{Al_2O_3}$ is the mass of alumina added and h_2 is the interfacial heat transfer coefficient as before. In order to test the hypothesis of heat transfer control, it is therefore necessary to determine the convective heat transfer coefficient for the electrolyte/alumina interface. This is the main aim of the quenching experiments.

If the heat flow calculated in Eq. 7 is divided by the instantaneous area of the frozen electrolyte layer on the cylinder, a spatially averaged heat flux profile is obtained. The flux profiles for the three cylinders are plotted against dimensionless time in Figure 5. As would be expected for experiments performed at the same superheat above the liquidus temperature, the curves coincide in most places although the process of taking temperature differentials introduces a random error because of the noisy response of the thermocouples in the liquid and in the crucible. The initial peak in the data is a result of turbulence caused by the quenching operation itself and is not relevant to the dissolution of alumina. Even so, the average heat flux incident on the immersed object for the remainder of the process is about 40,000 W · m^{-2}. In order to convert this value to a heat transfer coefficient the phase change temperature, T_L, must be determined.

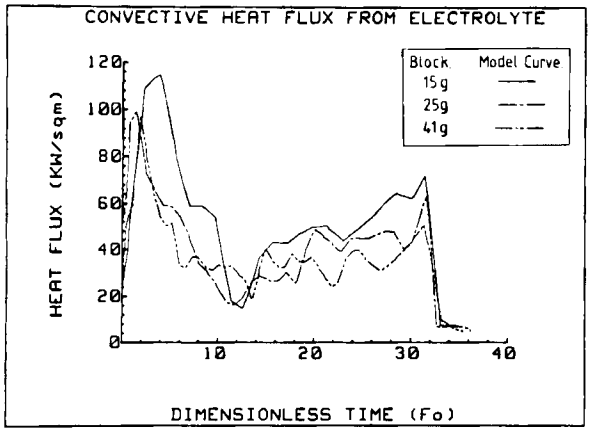

Figure 5. Convective heat flux incident on each cylinder during the phase change process.

A record of the radial and central temperatures of the 0.015 kg cylinder at the commencement of the quenching procedure is given in Figure 6a, and during the remelting process in Figure 6b. Reference to the radial thermocouple (T_4) in the skin of the block reveals that 100 s after immersion the rate of heating of the graphite surface increases abruptly and, as Figure 3 shows, this discontinuity in slope coincides with the disappearance of the frozen electrolyte layer. Similar surface temperature trends for the other blocks confirm that the phase change temperature during a rapid quench is 1,223 ± 3 K for an electrolyte of the stated composition. This is 18 K below the liquidus point and brings the convective temperature differential at the interface to 34 K. Adoption of this figure as the effective superheat of the electrolyte in Eq. 7 yields an average heat transfer coefficient of approximately 1,200 W · m^{-2} · K^{-1}. While this value is larger than the steady state estimate of Haupin (1971), it would be higher still if the theoretical liquidus point were used in the equation rather than the measured interface temperature, which is approaching the double solubility limit as indicated earlier.

Although the calculated coefficient is based on an interface temperature well below the actual liquidus, during alumina dissolution the surface temperature of the solid must be above this point if the process is to proceed. Gerlach (1983) measured the temperature of sintered alumina aggregates during dissolution,

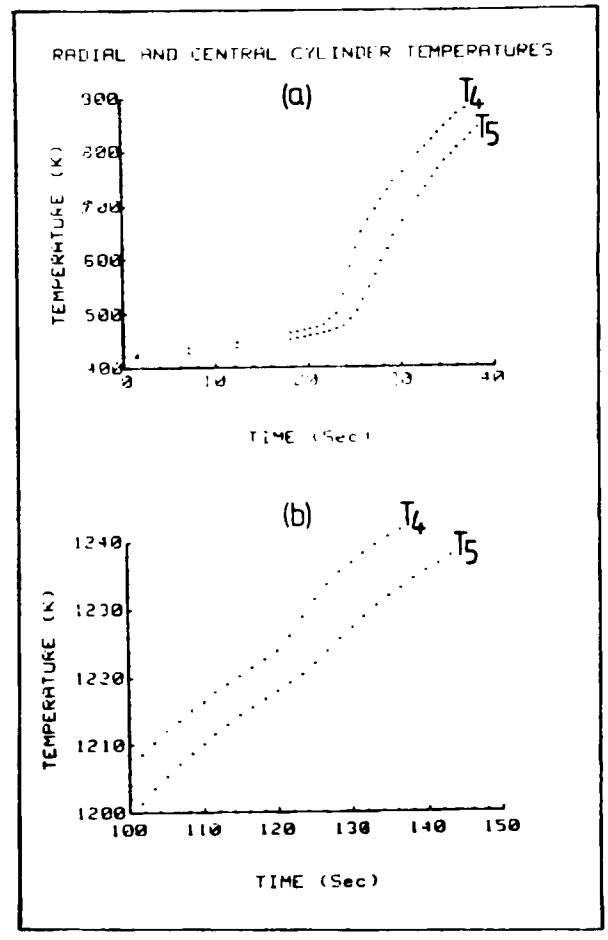

Figure 6. Radial (T_4) and central (T_5) thermocouple temperatures for the 0.015 kg cylinder.

a. During quenching
b. During final remelting

and his data indicate that the electrolyte/alumina temperature differential for alpha-alumina is approximately 10 K during dissolution. In addition, electrochemical measurements of alumina concentration (Jain et al., 1983a) during dissolution indicate that, for a 2 wt. % addition to a 0.75 kg stirred electrolyte, the initial rate of dissolution is $2.5–4.5 \times 10^{-4}$ kg · s^{-1}.

Under these conditions Eq. 10 predicts that for alpha-alumina ($\Delta H_{dissolution} = 1.95 \times 10^5$ J · mol^{-1}), aggregates of dissolving material larger than 300–400 μ dia. will be subject to heat transfer control. Since the average grain size of the commercially produced powder is around 80 μ, agglomeration of only 125 grains will cause the critical size to be reached. Even if the powder is uniformly dispersed in the melt, its initial concentration will be 5,000 grains per cubic centimeter and the probability of agglomeration is high. In practice the size distribution of the added alumina will allow fine particles (<50 μ) to dissolve quickly while aggregation of the $+100$ μ fraction is likely due to the localized addition of the powder to the electrolyte. The dissolving process from this point on could involve simultaneous electrolyte freezing and dissolution, possibly even on different areas of the same aggregate, until the particles either shrink below the critical size for heat transfer control or sink into the liquid aluminum pad as sludge. The extent of agglomeration will determine which of these possibilities occurs, emphasizing the importance of the alumina feeding technique in smelting cells.

Transient Heat Transfer at the Sidewall Ledge

The steady state and dynamic heat balances across the frozen ledge on the sidewall differ only in the latent energy flow that accompanies the freezing or melting of electrolyte. Also, it has been experimentally verified that gradual or steady freezing onto a vertical surface does not significantly alter the heat transfer coefficient between it and the adjacent fluid (Sparrow and Souza Mendes, 1982). For these reasons the transient convection from the electrolyte to the ledge interface should be proportional to the bulk temperature differential and the value of the heat transfer coefficient there.

Previous attempts by Arai and Yamazaki (1975) and Arita et al. (1978) to model the convective heat flow to the ledge surface ignored the ledge dynamics through overestimation of the electrolyte superheat; lack of experimental data on the convective heat transfer coefficient in cryolite-based systems has compounded the problem. Recent simulation of smelting cell convection by Solheim and Thonstad (1984), using biphenyl as a model liquid, yielded heat transfer coefficients in the 200–700 W · m^{-2} · K^{-1} range. Dernedde and Cambridge (1975) recommended the use of a correlation for forced convection over flat plates from which a value of 300 W · m^{-2} · K^{-1} can be calculated. However this method is highly suspect since the correlation applies only to fluids having Prandtl numbers approaching unity (gases only).

Excluding the effects of forced convection induced by anode gas release or liquid metal turbulence (Taylor and Welch, 1985), a theoretical analysis of free convection (Ostrach, 1953) at a vertical surface indicates that a 0.1 m section of ledge above the electrolyte/metal interface that allows unobstructed, downward liquid flow past it should experience an average heat transfer coefficient of 400–500 W · m^{-2} · K^{-1}. Although it is found that this is the position of minimum ledge protection on the sidewall, it has also been observed that any process disturbance resulting in a 10 K or more increase in electrolyte superheat instantly precipitates ledge melting at an average rate of approximately 1 mm per minute. The extent of the melting depends on the duration of the disturbance, but this phase change velocity is three times the figure predicted from the natural convection heat transfer coefficients given above. It is apparent from this that the heat transfer during extreme thermal transients is enhanced and approaches the value determined earlier in the quenching experiments.

Acknowledgment

The authors wish to express their appreciation to W. E. Haupin, Senior Fellow, Primary Products R and D, Aluminum Company of America, for helpful comments and criticisms during the course of this work. A. F. Mills, Department of Mechanical Engineering, University of Auckland, also made valuable suggestions on experimental techniques and data analysis. The authors also gratefully acknowledge the financial support for this project provided by the Process Metallurgy Division of Alcoa, New Kensington, Pennsylvania.

Notation

A = surface or interfacial area, m^2
Ac = surface area of a cylinder, m^2
As = surface area of a sphere, m^2
C = specific heat capacity, J · Kg^{-1} · K^{-1}
E = quantity of energy, J
Fo = Fourier number for immersed object
H = enthalpy of a lumped heat capacity, J
h = convective heat transfer coefficient, W · m^{-2} · K^{-1}
M = mass of a lumped heat capacity, kg
Q = heat flow, W
R = equivalent radius of cylinder, Eq. 1, m
r = radius of a cylinder, m
S = shape factor of immersed object, Eq. 2
T = temperature, K
t = time after object immersion in electrolyte, s
V = volume of a lumped heat capacity, m^3
α = thermal diffusivity, m^2 · s^{-1}
λ = latent heat of fusion, J · kg^{-1}
ρ = density of a lumped heat capacity, kg · m^{-3}

Subscripts

Al_2O_3 = alumina particles
d = total energy demand
L = phase change point
o = object preheat
s = latent energy supply

Literature Cited

Arai, K., and K. Yamazaki, "Heat Balance and Thermal Losses in Advanced Prebaked Anode Cells," *AIME Light Metals*, **1**, 193, (1975).

Archambault, P., and J. C. Chevrier, "Distribution de la Temperature au sein d'un Cylindre Trempe dans un Liquide Vaporisable," *Int. J. Heat Mass Transfer*, **20**, 1 (1977).

Arita, Y., N. Urata, and H. Ikeuchi, "Estimation of Frozen Bath Shape in an Aluminium Reduction Cell by Computer Simulation," *AIME Light Metals*, **1**, 59 (1978).

Bratland, D., K. Grjotheim, and C. Krohn, "Thermodynamic Discussion of Some Energy Problems in AL-Electrolysis," *AIME Light Metals*, **1**, 3 (1976).

Dernedde, E., and E. L. Cambridge, "Gas-Induced Circulation in an Aluminium Reduction Cell," *AIME Light Metals*, **1**, 111 (1975).

Gerlach, J., "Dissolution and Interaction between Alumina and Cryolite Melts," *1st Int. Symp. Molten Salt Chem. Tech., Japan*, 89 (1983).

Gerlach, J., U. Hennig, and K. Kern, "The Dissolution of Aluminium Oxide in Cryolite Melts," *AIME Light Metals*, **1**, 49 (1974).

Grjotheim, K., and B. J. Welch, *Aluminium Smelter Technology—A Pure and Applied Approach*, Aluminium Verlag, Dusseldorf, 95 (1980).

Haupin, W. E., "Calculating Thickness of Containing Walls Frozen from Melt," *AIME Light Metals,* **1,** 188 (1971).
Jain, R. K., M. P. Taylor, S. B. Tricklebank, and B. J. Welch, "A Study of the Relationship between the Properties of Alumina and its Interaction with Aluminium Smelting Electrolytes," *1st Int. Symp. Molten Salt Chem. Tech., Japan,* 59 (1983a).
Jain, R. K., S. B. Tricklebank, B. J. Welch, and D. J. Williams, "Interaction of Aluminas with Aluminium Smelting Electrolytes," *AIME Light Metals,* **1,** 609 (1983b).
Keller, R., "Alumina Dissolution and Sludge Formation," *AIME Light Metals,* **1,** 513 (1984).
Kent, J. H., "Attainment of High Current Efficiency on Aluminium-Reduction Furnaces by a Cold Running Technique," *J. Metals,* **22**(11), 30 (1970).
Lee, S. S., K. Lei, P. Xu, and J. J. Brown, "Determination of Melting Temperatures and Al_2O_3 Solubilities," *AIME Light Metals,* **1,** 841 (1984).
Noguchi, F., T., Nakamura, Y. Ueda, and T. Yanagase, "Mechanism of Al_2O_3 Dissolution into Cryolite Melt," *1st Int. Symp. Molten Salt Chem. Tech., Japan,* 13 (1983).
Ostrach, S., "An Analysis of Laminar Free-Convection Flow and Heat Transfer about a Flat Plate Parallel to the Direction of the Generating Body Force," NACA Report 1111 (1953).
Peacey, J. G., and G. W. Medlin, "Cell Sidewall Studies at Noranda Aluminium," *AIME Light Metals,* **1,** 475 (1979).
Schmidt-Hatting, W., "Investigations of Noise in Aluminium Electrolysis Cells," Metallurgical Soc. AIME, Paper No. A75-65, New York (1975).
Solheim, A., and J. Thonstad, "Model Experiments of Heat Transfer Coefficients between Bath and Side Ledge in Aluminium Cells," *J. Metals,* **36**(3), 51 (1984).
Sparrow, E. M., and P. Souza Mendes, "Natural Convection Heat Transfer Coefficients Measured in Experiments on Freezing," *Int. J. Heat Mass Transfer,* **25**(2), 293 (1982).
Tankin, R. S., and R. Farhadieh, "Effects of Thermal Convection Currents on Formation of Ice," *Int. J. Heat Mass Transfer,* **14,** 953 (1971).
Taylor, M. P., and B. J. Welch, "Bath/Freeze Heat Transfer Coefficients: Experimental Determination and Industrial Application," *AIME Light Metals,* **1,** 781 (1985).
Taylor, M. P., B. J. Welch, and J. T. Keniry, "Influence of Changing Process Conditions on the Heat Transfer During the Early Life of an Operating Cell," *AIME Light Metals,* **1,** 437 (1983a).
Taylor, M. P., B. J. Welch, and M. J. O'Sullivan, "Sidewall Ledge Dynamics in Cells Used for Electrowinning Aluminium," *Chemeca 83—Proc. 11th Aust. Chem. Eng. Conf.,* Brisbane, 493 (1983b).
Taylor, M. P., B. J. Welch, and J. T. Keniry, "The Effect of Electrochemical Changes on the Heat Balance in Aluminium Smelting Cells," *J. Electroanayltical Chem.,* **168,** 179 (1984).
Thonstad, J., P. Johanson, and E. W. Kristensen, "Some Properties of Alumina Sludge," *AIME Light Metals,* **1,** 227 (1980).
Thonstad, J., and S. Rolseth, "Equilibrium between Bath and Side Ledge in Aluminium Cells, Basic Principles," *AIME Light Metals,* **1,** 415 (1983).

Manuscript received June 11, 1985, and revision received Dec. 20, 1985.